ADVANCED MATERIALS
www.advmat.de

HOMO–HOMO Electron Transfer: An Elegant Strategy for p-Type Doping of Polymer Semiconductors toward Thermoelectric Applications

*Mahima Goel, Marie Siegert, Gert Krauss, John Mohanraj, Adrian Hochgesang, David C. Heinrich, Martina Fried, Jens Pflaum, and Mukundan Thelakkat**

Unlike the conventional p-doping of organic semiconductors (OSCs) using acceptors, here, an efficient doping concept for diketopyrrolopyrrole-based polymer PDPP[T]$_2$-EDOT (OSC-1) is presented using an oxidized p-type semiconductor, Spiro-OMeTAD(TFSI)$_2$ (OSC-2), exploiting electron transfer from HOMO$_{OSC\text{-}1}$ to HOMO$_{OSC\text{-}2}$. A shift of work function toward the HOMO$_{OSC\text{-}1}$ upon doping is confirmed by ultraviolet photoelectron spectroscopy (UPS). Detailed X-ray photoelectron spectroscopy (XPS) and UV–vis–NIR absorption studies confirm HOMO$_{OSC\text{-}1}$ to HOMO$_{OSC\text{-}2}$ electron transfer. The reduction products of Spiro-OMeTAD(TFSI)$_2$ to Spiro-OMeTAD(TFSI) and Spiro-OMeTAD is also confirmed and their relative amounts in doped samples is determined. Mott–Schottky analysis shows two orders of magnitude increase in free charge carrier density and one order of magnitude increase in the charge carrier mobility. The conductivity increases considerably by four orders of magnitude to a maximum of 10 S m^{-1} for a very low doping ratio of 8 mol%. The doped polymer films exhibit high thermal and ambient stability resulting in a maximum power factor of 0.07 µW m^{-1} K^{-2} at a Seebeck coefficient of 140 µV K^{-1} for a very low doping ratio of 4 mol%. Also, the concept of HOMO$_{OSC\text{-}1}$ to HOMO$_{OSC\text{-}2}$ electron transfer is a highly efficient, stable and generic way to p-dope other conjugated polymers.

Doped semiconductor polymers are gaining huge interest as materials in future energy conversion applications such as low-power polymeric thermoelectrics (TEs), because they are light weight, flexible, printable, and suitable for large area applications like wearable technologies.[1–4] The basic challenge in TE, however, lies in efficient doping of the organic semiconductors (OSCs), because OSCs have extremely low intrinsic charge carrier concentrations and hence very low electrical conductivities in the range of 10^{-6} to 10^{-12} S cm^{-1}. Molecular doping,[5] commonly used to increase the electrical conductivities of OSCs, involves the addition of a redox active organic or inorganic molecule as dopant. These dopants are capable of accepting (for p-type doping) or donating electrons to OSCs (for n-type doping), thereby generating free holes or electrons in OSCs. For p-type doping, acceptor dopants such as I_2,[6] $FeCl_3$,[7] molybdenum tris(1,2-bis(trifluoromethyl) ethane-1,2-dithiolene) (Mo(tfd)$_3$),[8] tetrafluorotetracyano-quinodimethane (F_4TCNQ) and its derivatives[9,10] have been extensively used. Although the precise mechanism of molecular doping in disordered semiconductors is still under discussion,[5,11,12] it is widely accepted that molecular doping involves either an integer charge transfer (ICT) or a ground state charge transfer complex (CPX) formation, followed by a charge separation in each case. In the more common ICT mechanism for polymers, an integer number of electrons is transferred from the highest occupied molecular orbital of the OSC (HOMO$_{osc}$) to the lowest unoccupied molecular orbital of the dopant (LUMO$_{dopant}$) during p-type doping, generating a coulombically bound electron hole pair. Since the HOMO energy levels of most OSCs are commonly in the range of 4.5–5.5 eV,[13] this process requires p-dopants with low lying LUMOs, which is challenging in terms of their synthesis and stability.[14,15] Moreover, as the dielectric constants of OSCs are low (often in the range of 3 to 4), the coulomb binding energy of the OSC cation and dopant anion pair is high, which lies in the range of 0.5–0.8 eV[16] and needs to be overcome to generate free charge carriers. This leads to poor doping efficiencies in OSCs and large amounts of dopants up to 30–40% percent are generally employed. However, theoretical results from Salzmann et al.[17] predict that the density of holes in the HOMO of the OSC reaches a maximum around 50% dopant concentration, at which the

Dr. M. Goel, G. Krauss, Dr. J. Mohanraj, A. Hochgesang, Dr. D. C. Heinrich, M. Fried, Prof. M. Thelakkat
Applied Functional Polymers
University of Bayreuth
Universitystr. 30, Bayreuth 95447, Germany
E-mail: mukundan.thelakkat@uni-bayreuth.de
M. Siegert, Prof. J. Pflaum
Experimental Physics VI
University of Würzburg
Am Hubland, Würzburg 97074, Germany
Prof. M. Thelakkat
Bavarian Polymer Institute
University of Bayreuth
Universitystr.30, Bayreuth 95447, Germany
The ORCID identification number(s) for the author(s) of this article can be found under https://doi.org/10.1002/adma.202003596.

DOI: 10.1002/adma.202003596

percentage of ionized dopants decreases below 10%, emphasizing the need to keep the dopant concentrations as low as possible. Moreover, doped systems obtained using acceptor dopants such as F_4TCNQ usually suffer from stability issues.

These general limitations of conventional redox doping led us to a new concept of doping by mixing two p-type semiconductors (OSC-1 and OSC-2): OSC-1 being a pristine (non-doped) semiconductor polymer and major component, and OSC-2 a chemically oxidized semiconductor (low mol. wt. molecule and minor component), which can function as a dopant for OSC-1. Here, the electrons can be transferred from the fully occupied $HOMO_{OSC\text{-}1}$ of the polymer to the partly occupied $HOMO_{OSC\text{-}2}$. This partly filled HOMO is most probably a singly occupied molecular orbital (SOMO) as in radicals, but the term SOMO is here not specifically used due to the fact that the presence of unpaired electron is not proven. Thus, electron transfer features a $HOMO_{OSC\text{-}1}$ to $HOMO_{OSC\text{-}2}$ type transition rather than the conventional $HOMO_{osc}$–$LUMO_{dopant}$ type process, and therefore no dopants with extremely low LUMOs are required.

For this purpose, we selected the well-known hole conductor Spiro-OMeTAD$(TFSI)_2$, a chemically oxidized radical cation salt of pristine 2,2′,7,7′-tetrakis(*N*,*N*-di-*p*-methoxyphenylamine)-9,9′-spirobifluorene (Spiro-OMeTAD) as OSC-2, which has a partly filled HOMO to serve as p-type dopant. It is to be noted that Spiro-OMeTAD$(TFSI)_2$ has been known as an additive to Spiro-OMeTAD from the earlier works of Cappel et al.[18] and Nguyen et al.[19] to improve its electrical conductivity when employed in hole transport layers in solar cells. In our approach, we expect that Spiro-OMeTAD$(TFSI)_2$ may get reduced to Spiro-OMeTAD(TFSI) or Spiro-OMeTAD upon doping the polymer, and the resulting doped system becomes a mixture of two or more hole conductors. Additionally, charge delocalization in conjugated polymer chains can be favorable for charge transport. Since, no new acceptor anions/or radical anions are formed as a result of doping in addition to the highly stable TFSI anion already present, a potential improvement in the thermal and air stability of doped films are also expected. All these factors may give added advantage to the overall electrical conductivity/charge transport of the system and a possibility of reaching the saturation conductivity at much lower concentrations of the dopant.

To check the validity of our doping strategy, we chose a diketopyrrolopyrrole-based PDPP[T]$_2$-EDOT polymer[20] (IP = −4.49 eV), such that its HOMO lies above the HOMO of Spiro-OMeTAD$(TFSI)_2$ (IP = −5.33 eV). The main questions that we have addressed to answer in this communication are: a) Is electron transfer possible between a PDPP[T]$_2$-EDOT (OSC-1) and Spiro-OMeTAD$(TFSI)_2$ (OSC-2), resulting in higher electrical conductivity than Spiro-OMeTAD$(TFSI)_2$?, b) What is the optimum Spiro-OMeTAD$(TFSI)_2$ concentration required to reach the saturation conductivity and can it be kept low compared to the conventional acceptor dopants such as F_4TCNQ?, c) What is the consequence of such a HOMO–HOMO charge transfer on charge carrier concentration, carrier mobility, electrical conductivity, stability and thermoelectric properties of the doped polymer films? and d) Can Spiro-OMeTAD$(TFSI)_2$ be successfully used as a generic dopant for other classes of p-type polymers?

The chemical structures of the investigated diketopyrrolopyrrole-based polymer PDPP[T]$_2$-EDOT (OSC-1), Spiro-OMeTAD$(TFSI)_2$ (OSC-2) and Spiro-OMeTAD are shown in **Figure 1**. PDPP-[T]$_2$-EDOT (M_n = 19 420 g mol^{-1}; T_m = 334 °C in flash DSC at 200 K s^{-1}) and Spiro-OMeTAD$(TFSI)_2$ were synthesized using procedures known in the literature and described in the Supporting Information.[19–22] Spiro-OMeTAD$(TFSI)_2$ was characterized using X-ray photoelectron spectroscopy (XPS) and UV–vis spectroscopy. See Figures S1 and S2 in the Supporting Information for its atomic and chemical composition. Detailed XPS studies (Figures S3 to S5, Supporting Information) showed that upon addition of ≈1, 2, and 9 mol% of Spiro-OMeTAD$(TFSI)_2$ into PDPP[T]$_2$-EDOT, the maxima of the N1s and S2p peaks of the latter slightly shifted to a higher binding energy region of 400.3 eV (from 399.8 eV) and 164.4 eV (from 163.9 eV), respectively, indicating the oxidation of the polymer backbone, i.e., an electron transfer from PDPP[T]$_2$-EDOT to Spiro-OMeTAD$(TFSI)_2$ (Figure S5, Supporting Information).[23,24]

While XPS studies give indications of the electron transfer interactions between PDPP[T]$_2$-EDOT and Spiro-OMeTAD$(TFSI)_2$, a quantitative assessment of p-doping on the electronic energy levels of the polymer was obtained using UPS. As derived from the valence band maximum and secondary electron cut-off (Figure 1b), the work function and ionization energy of the pristine polymer corresponds to 4.49 and 3.90 eV, whereas Spiro-OMeTAD$(TFSI)_2$ exhibits −5.33 and −5.06 eV, respectively. Details of the ionization energies, work functions (E_F) and the hole injection barriers (HIBs) for differently doped samples (0.97, 2.01, 8.99, and 13.83 mol%) are collected in Table S1 (Supporting Information). It can be seen that the E_F of the polymer is shifted from −3.90 down to −4.77 eV, whereas the ionization energy is stabilized at ≈−4.8 eV. An initial change of 240 meV in the HIB at ≈0.99 mol% of Spiro-OMeTAD$(TFSI)_2$ indicates a high trap density in the polymer matrix.[17,25] As shown in Figure 1c, further increasing the dopant ratio leads to a steady decrease of the HIB from 590 meV (in pristine) down to 60 meV (for 13.83 mol% dopant concentration), virtually merging the HOMO of the polymer with E_F. Such a shift of the HOMO toward E_F ascertains unambiguously p-doping the PDPP[T]$_2$-EDOT. Further, a linear approximation of work function and HIB exhibits a slope of $\approx 10 k_B T$ across the entire concentration range, a value higher than $k_B T$, commonly observed due to dopant induced disorder in the organic matrix (Figure S6, Supporting Information).[26] Similarly, a relative broadening of the occupied valence states, i.e., FWHM of the Gaussian peak from 1.11 eV for pristine PDPP[T]$_2$-EDOT to 1.54 eV for 13.83 mol% of the Spiro-OMeTAD$(TFSI)_2$-doped system (Figure S7, Supporting Information) confirmed the formation of new states due to the oxidation of the polymer matrix or reduction of the dopant, which contributes to the valence states. These observations clearly indicate the highly efficient p-doping capability of Spiro-OMeTAD$(TFSI)_2$ toward PDPP[T]$_2$-EDOT.

UV–vis–NIR absorption spectroscopy was used to characterize the absorption features of doping induced novel species and thus to quantify the doping process. The absorption spectra of pristine PDPP[T]$_2$-EDOT polymer, and doped samples are given in **Figure 2**a and the concentrations are tabulated in Table S2 (Supporting Information). Pristine PDPP[T]$_2$-EDOT exhibits main absorption peaks/shoulders at 440, 860, and 955 nm. As the doping progresses, a decrease in the intensities of the absorption bands of the neutral polymer and a concomitant increase in intensities of the new absorption features at about 1100 nm were observed, confirming charge transfer. Spectro-electrochemical (SEC) measurements (Figure 2c) were used to assign the new absorption band

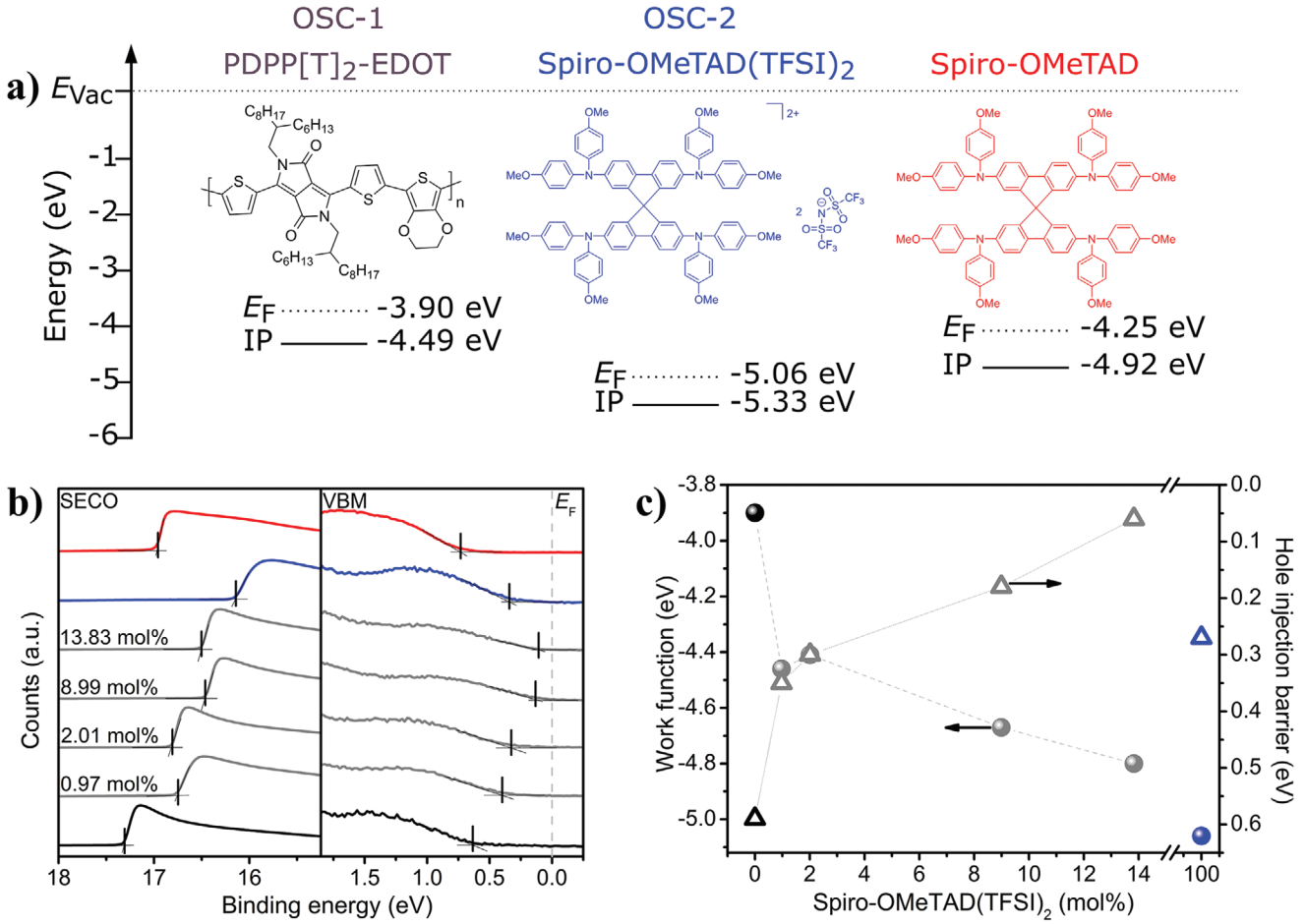

Figure 1. a) Chemical structures of PDPP[T]$_2$-EDOT (OSC-1), Spiro-OMeTAD(TFSI)$_2$(OSC-2) and Spiro-OMeTAD, and schematic diagrams of the corresponding Fermi- and occupied frontier energy levels, measured by UPS. b) Photoemission spectra showing the secondary electron cut-off SECO (left) and valence band maximum VBM (right) regions of OSC-1 (black), doped samples (gray), OSC-2 (blue) and pristine spiro-OMeTAD (red), scaled with respect to the Fermi energy level (E_F: vertical gray dashed line set at zero eV). c) Variation of the work function (black and gray spheres) and hole injection barriers HIB (triangles) of OSC-1 upon doping with OSC-2 as well as the values for OSC-2 (blue) derived from UPS measurements. The lines in (c) are guidelines for the eye.

to polaronic (oxidized species) absorption at 1100 nm. The small differences in peak positions between SEC spectra and absorption of chemically doped samples (Figure 2b,c) arise from the different degrees of oxidation and polarity differences in the medium in both methods. See details of SEC plots under different conditions in Figure S8 (Supporting Information).

To fundamentally understand the reduction of the Spiro-OMeTAD(TFSI)$_2$ during the oxidation of PDPP[T]$_2$-EDOT, difference spectra (ΔA) (Figure 2b) were plotted by subtracting the absorption spectrum of the pristine polymer from the absorption spectra of the doped samples. The magnified part (300–600 nm) of this, shown in Figure 2d corresponds mainly to the various reduced dopant species since the change in absorption of oxidized polymer species in this range is negligible as shown in SEC studies. Comparing the ΔA spectra with the absorption spectra of Spiro-OMeTAD(TFSI)$_2$ and Spiro-OMeTAD, (shown in Figure 2d) gives a clear indication that pristine Spiro-OMeTAD is formed during doping. However, Figure 2d alone cannot differentiate the formation of relative amounts of each species. In order to estimate the relative amounts of the Spiro-OMeTAD, Spiro-OMeTAD(TFSI), and the unreacted Spiro-OMeTAD(TFSI)$_2$ present in doped polymer solutions at different doping concentrations, we used reported molar extinction coefficients[19] of Spiro-OMeTAD at 390 nm, Spiro-OMeTAD(TFSI) and Spiro-OMeTAD(TFSI)$_2$ at 390, 480, and 520 nm respectively. The molar concentrations of each species were then calculated using Beer-Lambert law. Details are shown in the Figure S9 and Table S3 (Supporting Information). As can be seen in Figure S9 (Supporting Information), the slope of concentration plot for Spiro-OMeTAD(TFSI) is the highest, indicating a rapid increase in the concentration of Spiro-OMeTAD(TFSI) compared to the other two species. Additionally, the sum of the relative concentration of the reduced products (Spiro-OMeTAD(TFSI) and Spiro-OMeTAD) saturates around 70% (Table S3, Supporting Information). This clearly confirms a $HOMO_{OSC\text{-}1}$ to $HOMO_{OSC\text{-}2}$ electron transfer from PDPP[T]$_2$-EDOT to Spiro-OMeTAD(TFSI)$_2$ and its reduction from +2 to +1 as well as to the pristine state. A similar doping pattern was also observed in the absorption spectra of solid thin films (Figure S10, Supporting Information). The high ambient

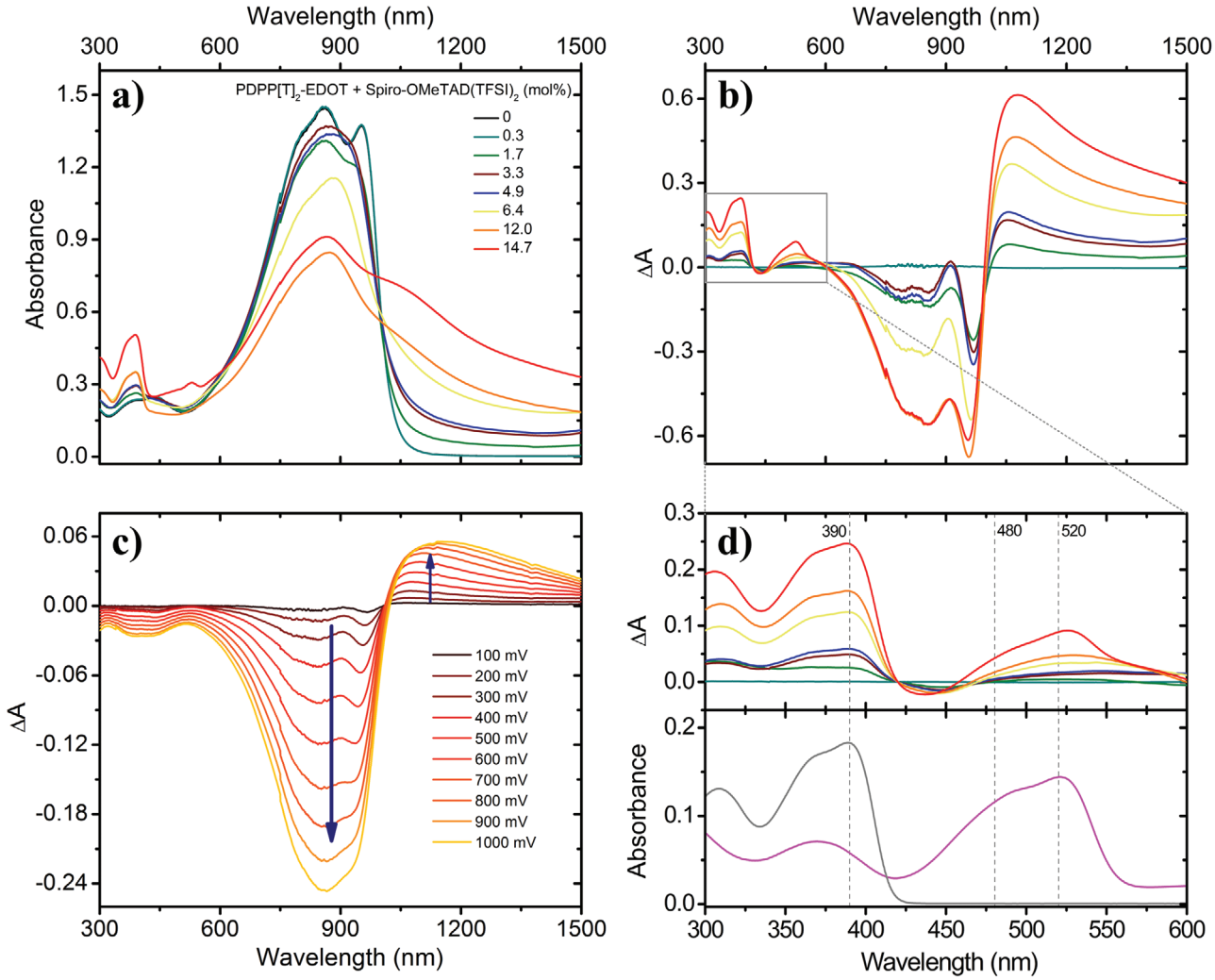

Figure 2. a) Absorption spectra of pristine and doped PDPP[T]$_2$-EDOT solutions at different concentrations of Spiro-OMeTAD(TFSI)$_2$. b) Absolute changes in the absorption spectra obtained by subtracting the absorption spectrum of the neutral polymer from the absorption spectra of the doped polymer solutions. c) Differential spectro-electrochemical UV–vis–NIR plots of neat PDPP[T]$_2$-EDOT in solution. d) Expanded absorption spectra of 2b from the region 300 to 600 nm along with the absorption of Spiro-OMeTAD(TFSI)$_2$ (shown in magenta), and Spiro-OMeTAD (shown in gray).

stability of the doped polymer solutions and films was confirmed by the persistence of the absorption spectra during five days under inert atmosphere and afterward in air (Figure S11, Supporting Information).

In order to evaluate the consequences of doping PDPP[T]$_2$-EDOT with Spiro-OMeTAD(TFSI)$_2$, the charge carrier density (N_D) was calculated from the Boltzmann corrected Mott–Schottky equation (Equation (1)) for capacitance-voltage measurements on metal-insulator-semiconductor (MIS) devices at RT (Figure S12 and Table S4, Supporting Information)[27] using impedance spectroscopy (**Figure 3**a and Tables S5 and S6 in the Supporting Information for details)

$$\frac{1}{C_{tot}^{\ 2}} = \frac{2}{q\varepsilon_0\varepsilon_{OSC}A^2N_D}\left(V_{Fb} - V_{Bias} - \frac{k_BT}{q}\right) \quad (1)$$

where C_{tot} is the total capacitance obtained from the impedance, q is the elementary charge, ε_0 and ε_{OSC} are the dielectric constants of the vacuum and the organic layer (≈3), A the active area, V_{Fb} the flat band voltage, V_{Bias} the applied bias voltage, k_B the Boltzmann constant and T the junction temperature.

Also, the zero field mobility of majority charge carriers (μ_0) was calculated by extrapolating the obtained Poole–Frenkel type field dependency (Equation (2)) in conjunction with negative differential susceptance measurements ($-\Delta B$) of metal-semiconductor (MS) devices (Figure 3a and Table S7 (Supporting Information) for details)

$$\mu = \frac{4}{3}\frac{d^2}{\tau_t V_{Bias}} \quad (2)$$

where τ_t is the transit time obtained from ($-\Delta B$) measurements and d being the thickness of the organic layer.

The pristine polymer PDPP[T]$_2$-EDOT exhibits N_D of 9.80 ± 3.09 × 10^{19} cm^{-3}, which increases to a maximum of 8.81 ± 3.77 × 10^{21} cm^{-3}, when doped with 4.74 mol% of

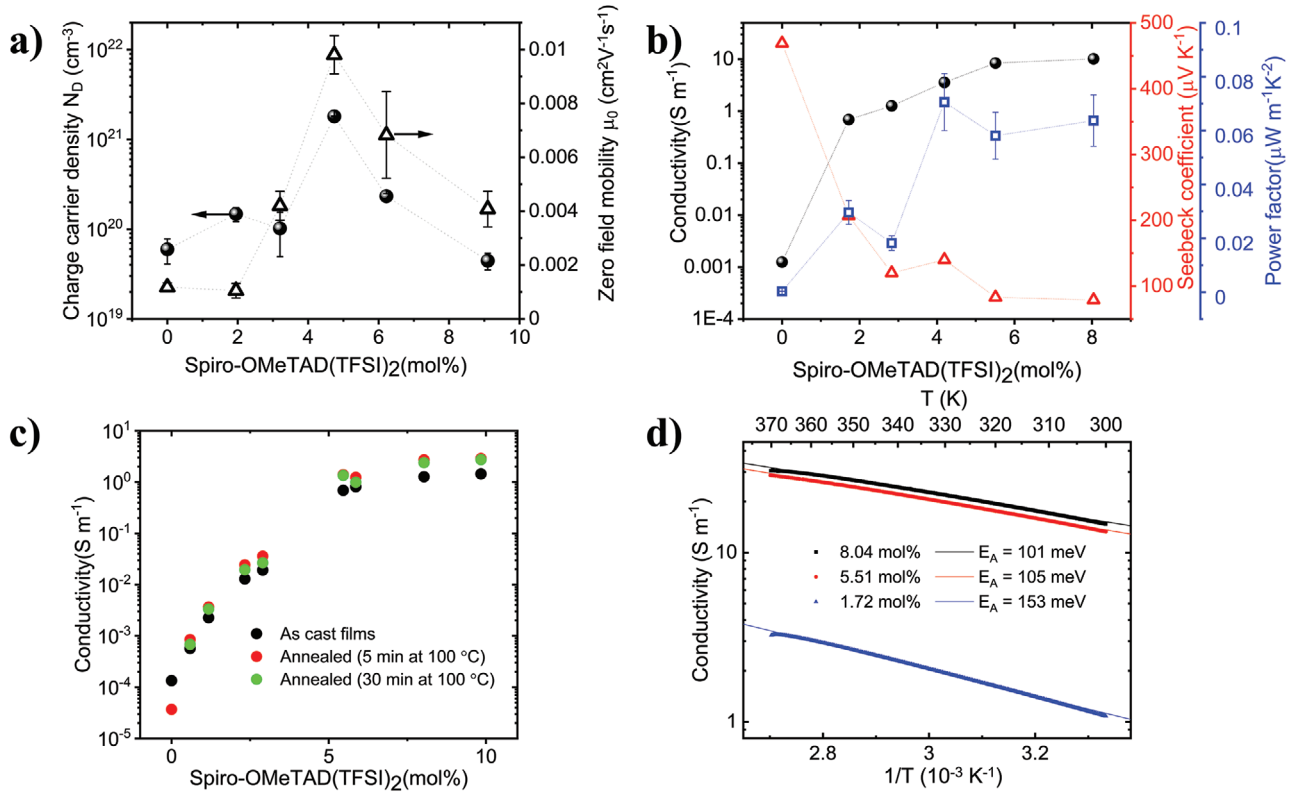

Figure 3. a) Charge carrier density N_D (circles) and zero-field mobility μ_0 (triangles) of PDPP[T]$_2$-EDOT (OSC-1) doped with Spiro-OMeTAD(TFSI)$_2$ (OSC-2). b) Electrical conductivity (σ) (black), Seebeck coefficient (S) (red), and corresponding power factor (PF = σS^2) (blue) as function of Spiro-OMeTAD(TFSI)$_2$ concentration at room temperature, c) Temperature stability of conductivity for doped samples: as-prepared films (black), annealed at 100 °C for 5 mns (red) and annealed at 100 °C for 30 mns (green) in a glovebox and d) temperature-dependent conductivity measurements in the range of 300 to 370 K on samples with doping concentrations of 1.72 mol% (blue), 5.51 mol% (red), and 8.04 mol%(black). From Arrhenius fits, the activation energies of 153, 105, and 101 meV respectively were obtained.

Spiro-OMeTAD(TFSI)$_2$. Similarly, μ_0 increased from $1.18 \pm 0.16 \times 10^{-3}$ to $9.81 \pm 0.71 \times 10^{-3}$ cm^2 V^{-1} s^{-1}, until it starts decreasing at higher concentrations of Spiro-OMeTAD(TFSI)$_2$. A general trend of increasing N_D and μ_0 was observed up to 5 mol% of Spiro-OMeTAD(TFSI)$_2$. A deterioration in the electronic transport properties (N_D and μ_0) above 5 mol% can be attributed to increased static disorder or precipitation of the active dopant.[28] Although Arkhipov et al.[16] predicted that an initial decrease in the mobility could occur due to doping-induced coulombic disorder, we could not observe this behavior because the zero-field mobilities for 0 and 2 mol% Spiro-OMeTAD(TFSI)$_2$ lie well within each other's error margin. Using Pasveer's theory, the DOS width of doped PDPP[T]$_2$-EDOT can be estimated as ≈126 meV at 3.3 mol% of Spiro-OMeTAD(TFSI)$_2$, which proves the high level of disorder in our investigated system.[29] Thus impedance studies confirm the increase in charge carrier density as well as the mobility.

Furthermore, electrical conductivity, Seebeck coefficient and resulting power factor (PF = σS^2) of PDPP[T]$_2$-EDOT films with varying Spiro-OMeTAD(TFSI)$_2$ concentrations were measured as shown in Figure 3b and all values are collected in Table S8 (Supporting Information). The conductivities of the doped films increased by four orders of magnitude from 1.25×10^{-3} S m^{-1} for the pristine PDPP[T]$_2$EDOT to a maximum of 10.21 S m^{-1}, with a saturation in conductivity attained around 5 mol% of Spiro-OMeTAD(TFSI)$_2$ in PDPP[T]$_2$EDOT films. It is to be noted that this saturation value is more than two orders of magnitude higher than the measured value for pure Spiro-OMeTAD(TFSI)$_2$ (σ = 5.41 ×10^{-2} S m^{-1}), indicating the additional contribution of doped conjugated polymers toward σ via delocalization of charges. A comparison with other literature reports on F$_4$TCNQ-doped polymers such as PDPP(6-DO)2TT (σ_{max} = 6.4 × 10^{-2} S m^{-1} at a molar doping ratio = 0.33)[30] or P3HT-PEO blends (σ_{max} = 84.7 S m^{-1} at mol% = 20)[31] reflect that, with Spiro-OMeTAD(TFSI)$_2$ a saturation conductivity of 10.21 S m^{-1} could be reached using quite low amounts of dopant. As expected for a molecular doping process, the measured conductivity σ rises steeply upon trap-filling. Further introduction of the dopant leads to dopant saturation and eventually dopant reserve, causing σ to asymptotically approximate a steady value.[32] This behavior was also verified by measuring conductivity through *IV*-curve tracing of planar, interdigitated electrode structures. The high thermal and air stability of the doped conducting polymer films was confirmed by the excellent retention of electrical conductivity after annealing at 100 °C as well as exposing the samples to air (Figure 3c and Figure S13, Supporting Information). We assume that the absence of any acceptor radical anions as in the case of F$_4$TCNQ-doped systems contribute strongly toward the thermal and ambient stability. The Seebeck coefficients of the

doped polymer films were measured (Figure 3b and Figure S14, Supporting Information) to estimate their power factor ($PF = \sigma S^2$). The Seebeck coefficients gradually decreased from 469 μV K^{-1} for the pristine PDPP[T]$_2$EDOT film to 79 μV K^{-1} as the amount of Spiro-OMeTAD(TFSI)$_2$ increased to 8.04 mol%. This reciprocal interdependence of σ and S agrees with theoretical descriptions of charge carrier transport in organic semiconductors based on an effective transport band model yielding Equation (3)[33]

$$S = -\frac{k_B}{q}\int_{-\infty}^{\infty}\frac{(E-E_F)}{k_BT}\frac{\sigma(E)}{\sigma}dE \quad (3)$$

Here, q refers to the elementary charge, E_F to the Fermi-energy and $\sigma(E)$ to the electrical conductivity for a given energy E within the transport band. However, depending on the respective density of states for a given polymer as well as on its energetic disorder, the Seebeck-coefficient does not necessarily scale inversely proportional to σ but rather as $S \approx \sigma^{x}$, with $0 < x < 1$. Fitting the experimental Seebeck data as a function of σ reveals the relation $S \approx \sigma^{-0.2}$ (Figure S15, Supporting Information), which is in line with the previously reported empirical power law $S \approx \sigma^{-0.25}$ for doped polymeric semiconductors.[34] In good agreement with this empirical model, the corresponding Power Factor PF is found to increase with $\sigma^{0.6}$.

As depicted in Figure 3b, the power factor increases with higher doping concentrations from 0.0003 μW m^{-1} K^{-2} for the undoped polymer to reach its maximum of about 0.07 μW m^{-1} K^{-2} at an intermediate Spiro-OMeTAD(TFSI)$_2$ doping concentration of 4.19 mol%. The trade-off between the increase in conductivity and the decrease in Seebeck coefficient results in a net improvement of two orders of magnitude in PF as shown in Figure 3b. Temperature dependent conductivity measurements (Figure 3d) revealed an increase in electrical conductivity with temperature. The charge carrier activation energy E_A has been extracted by fitting the data according to Equation (4). As can been seen by the semi-logarithmic plot of $\sigma(1/T)$ in Figure 3d, for all samples the electrical conductivity shows an increase with temperature according to an Arrhenius-type behavior that can be described by

$$\sigma(T) = \sigma_0 \exp\left(-\frac{E_A}{k_BT}\right) \quad (4)$$

with σ_0: saturation conductivity at high temperatures, E_A: thermal activation energy of charge carrier transport, T: absolute temperature and k_B: Boltzmann constant. The activation energies decrease toward higher doping concentrations from (153 ± 19) meV at 1.72 mol% of Spiro-OMeTAD(TFSI)$_2$ to (101 ± 8) meV at 8.04 mol%, due to the incremental filling of the Gaussian-distributed density of states (DOS) accompanied by an increase in contributing transport states.

We also tested if this concept of HOMO–HOMO electron transfer using Spiro-OMeTAD(TFSI)$_2$ can be extended to other common semiconductor polymers such as P3HT and a soluble PEDOT derivative (Figure S16, Supporting Information), in order to widen the applicability and scope of this strategy. Our preliminary results show that this concept has general validity and the electrical conductivities of P3HT and PEDOT increased from 3.33×10^{-4} to 8.99×10^{-1} S m^{-1} and from 9.12×10^{-4} to 1.28×10^{-1} S m^{-1}, respectively, upon doping. Further detailed doping studies of P3HT and PEDOT using Spiro-OMeTAD(TFSI)$_2$ are currently under investigation.

In summary, we demonstrated a highly efficient p-doping strategy for the diketopyrrolopyrrole-based PDPP[T]$_2$-EDOT polymer (OSC-1) by mixing with another p-type semiconductor Spiro-OMeTAD(TFSI)$_2$ (OSC-2), achieving a HOMO to HOMO electron transfer from OSC-1 to OSC-2. The doping was confirmed by the gradual shift of the E_F toward polymer HOMO upon adding Spiro-OMeTAD(TFSI)$_2$ using UPS analysis. The evidences for p-doping via electron transfer from $HOMO_{OSC\text{-}1}$ to $HOMO_{OSC\text{-}2}$ were corroborated using XPS, SEC and UV–vis–NIR studies. Mott–Schottky analysis of impedance measurements on MIS devices exhibited two orders of magnitude increase in free charge carrier density with a maximum N_D of $8.81 \pm 3.77 \times 10^{21}$ cm^3. Similarly, zero-field mobility (μ_0) of the pristine polymer increased from 1.18×10^{-3} to 9.81×10^{-3} cm^2 V^{-1} s^{-1}. The electrical conductivities of the doped films showed four orders of magnitude increase from 1.25×10^{-3} S m^{-1} for the pristine PDPP[T]$_2$-EDOT to a maximum of 10.21 S m^{-1}. Both, the electrical conductivity and the Seebeck measurements confirmed the high stability of the doped polymer films upon thermal annealing as well as upon exposing the films to air. This is a major advantage of doping OSC-1 with OSC-2. Finally, a maximum power factor of 0.07 μW m^{-1} K^{-2} was reached at a Seebeck coefficient value of 140 μV K^{-1} for a doping ratio of 4.19 mol%. The general validity of this doping concept was demonstrated by employing Spiro-OMeTAD(TFSI)$_2$ as dopant for other classes of polymers such as PEDOT and P3HT. This innovative doping approach enables the use of a wide variety of doped hole conductors as dopants as well as blend components without the requirement of any additional acceptor molecules with low LUMO values.

Supporting Information

Supporting Information is available from the Wiley Online Library or from the author.

Acknowledgements

Bavarian State Ministry for Education, Science and the Arts (Project: SolTech) is acknowledged for financial support. Also, the XPS/UPS facility (PHI 5000 VersaProbe III system) at Keylab Device Engineering in Bavarian Polymer Institute, University of Bayreuth is acknowledged. M.S. gratefully acknowledges financial support by the Deutsche Bundesstiftung Umwelt.

Open access funding enabled and organized by Projekt DEAL.

Conflict of Interest

The authors declare no conflict of interest.

Keywords

molecular doping, Mott–Schottky analysis, organic semiconductors, polymer thermoelectrics, ultraviolet photoelectron spectroscopy

Received: May 26, 2020
Revised: July 20, 2020
Published online: September 18, 2020

[1] A. C. Arias, J. D. MacKenzie, I. McCulloch, J. Rivnay, A. Salleo, *Chem. Rev.* **2010**, *110*, 3.
[2] H. M. Elmoughni, A. K. Menon, R. M. W. Wolfe, S. K. Yee, *Adv. Mater. Technol.* **2019**, *4*, 1800708.
[3] B. Russ, A. Glaudell, J. J. Urban, M. L. Chabinyc, R. A. Segalman, *Nat. Rev. Mater.* **2016**, *1*, 16050.
[4] M. Goel, M. Thelakkat, *Macromolecules* **2020**, *53*, 3632.
[5] I. E. Jacobs, A. J. Moulé, *Adv. Mater.* **2017**, *29*, 1703063.
[6] C. J. Boyle, M. Upadhyaya, P. Wang, L. A. Renna, M. Lu-Díaz, S. P. Jeong, N. Hight-Huf, L. Korugic-Karasz, M. D. Barnes, Z. Aksamija, D. Venkataraman, *Nat. Commun.* **2019**, *10*, 2827.
[7] Z. Liang, M. J. Boland, K. Butrouna, D. R. Strachanb, K. R. Graham, *J. Mater. Chem. A* **2017**, *5*, 15891.
[8] Y. Qi, T. Sajoto, S. Barlow, E.-G. Kim, J. -L. Bre´das, S. R. Marder, A. Kahn, *J. Am. Chem. Soc.* **2009**, *131*, 12530.
[9] D. Kiefer, R. Kroon, A. I. Hofmann, H. Sun, X. Liu, A. Giovannitti, D. Stegerer, A. Cano, J. Hynynen, L. Yu, Y. Zhang, D. Nai, T. F. Harrelson, A. J. M. M.Sommer, M. Kemerink, S. R. Marder, I. McCulloch, M. Fahlman, S. Fabiano, C. Müller, *Nat. Mater.* **2019**, *18*, 149.
[10] P. Pingel, D. Neher, *Phys. Rev. B* **2013**, *87*, 115209.
[11] M. L. Tietze, J. Benduhn, P. Pahner, B. Nell, M. Schwarze, H. Kleemann, M. Krammer, K. Zojer, K. Vandewal, K. Leo, *Nat. Commun.* **2018**, *9*, 1182.
[12] A. Mityashin, T. V. R. Y.Olivier, C. Rolin, S. Verlaak, N. G. Martinelli, D. Beljonne, J. Cornil, J. Genoe, P. Heremans, *Adv. Mater.* **2012**, *24*, 1535.
[13] J. Chen, Y. Cao, *Acc. Chem. Res.* **2009**, *42*, 1709.
[14] J. Saska, G. Gonel, Z. I. Bedolla-Valdez, S. D. Aronow, N. E. Shevchenko, A. S. Dudnik, A. J. Moulé, M. Mascal, *Chem. Mater.* **2019**, *31*, 1500.
[15] V. A. Kolesov, C. F.-H., W.-F. Chou, N. Aizawa, F. A. Larrain, A. P. M.Wang, S. Choi, S. Graham, G. C. Bazan, T.-Q. Nguyen, S. R. Marder, B. Kippelen, *Nat. Mater.* **2017**, *16*, 474.
[16] V. I. Arkhipov, P. Heremans, E. V. Emelianova, H. Bässler, *Phys. Rev. B* **2005**, *71*, 045214.
[17] I. Salzmann, G. Heimel, M. Oehzelt, S. Winkler, N. Koch, *Acc. Chem. Res.* **2016**, *49*, 370.
[18] U. B. Cappel, T. Daeneke, U. Bach, *Nano Lett.* **2012**, *12*, 4925.
[19] W. H. Nguyen, C. D. Bailie, E. L. Unger, M. D. McGehee, *J. Am. Chem. Soc.* **2014**, *136*, 10996.
[20] C. J. Mueller, C. R. Singh, M. Thelakkat, *J. Polym. Sci., Part B: Polym. Phys.* **2016**, *54*, 639.
[21] C. J. Mueller, E. Gann, C. R. Singh, M. Thelakkat, C. R. McNeill, *Chem. Mater.* **2016**, *28*, 7088.
[22] B. Tan, S. R. Raga, A. S. R. Chesman, S. O. Fürer, F. Zheng, D. P. McMeekin, L. Jiang, W. Mao, X. Lin, X. Wen, J. Lu, Y.-B. Cheng, U. Bach, *Adv. Energy Mater.* **2019**, *9*, 1901519.
[23] R. Schölin, M. H. Karlsson, S. K. Eriksson, H. Siegbahn, E. M. J. Johansson, H. Rensmo, *J. Phys. Chem. C* **2012**, *116*, 26300.
[24] C. G. Wu, Y. R. Yeh, L. N. Chien, *Polymer* **2000**, *41*, 5839.
[25] M. L. Tietze, L. Burtone, M. Riede, B. Lüssem, K. Leo, *Phys. Rev. B* **2012**, *86*, 035320.
[26] S. Olthof, W. Tress, R. Meerheim, B. Lüssem, K. Leo, *J. Appl. Phys.* **2009**, *106*, 103711.
[27] K. Gelderman, L. Lee, S. W. Donne, *J. Chem. Educ.* **2007**, *84*, 685.
[28] M. Schwarze, C. Gaul, R. Scholz, F. Bussolotti, A. Hofacker, K. S. Schellhammer, B. Nell, B. D. Naab, Z. Bao, D. Spoltore, K. Vandewal, J. Widmer, S. Kera, N. Ueno, F. Ortmann, K. Leo, *Nat. Mater.* **2019**, *18*, 242.
[29] R. Coehoorn, W. F. Pasveer, P. A. Bobbert, M. A. J. Michels, *Phys. Rev. B* **2005**, *72*, 155206.
[30] Y. Karpov, T. Erdmann, I. Raguzin, M. Al-Hussein, M. Binner, U. Lappan, M. Stamm, K. L. Gerasimov, T. Beryozkina, V. Bakulev, D. V. Anokhin, D. A. Ivanov, F. Günther, S. Gemming, G. Seifert, B. Voit, R. D. Pietro, A. Kiriy, *Adv. Mater.* **2016**, *28*, 6003.
[31] D. Kiefer, L. Yu, E. Fransson, A. Gómez, D. Primetzhofer, A. Amassian, M. Campoy-Quiles, C. Müller, *Adv. Sci.* **2017**, *4*, 1600203.
[32] M. L. Tietze, P. Pahner, K. Schmidt, K. Leo, B. Lüssem, *Adv. Funct. Mater.* **2015**, *25*, 2701.
[33] G. Kim, K. P. Pipe, *Phys. Rev. B* **2012**, *86*, 085208.
[34] A. M. Glaudell, J. E. Cochran, S. N. Patel, M. L. Chabinyc, *Adv. Energy Mater.* **2015**, *5*, 1401072.